Effect analysis of bearing and interface dynamics on tool point FRF for chatter stability in machine tools by using a new analytical model for spindle–tool assemblies

A. Ertürk[a], H.N. Özgüven[a], E. Budak[b],*

[a]Department of Mechanical Engineering, Middle East Technical University, 06531 Ankara, Turkey
[b]Faculty of Engineering and Natural Sciences, Sabanci University, Orhanli, Tuzla, 34956 Istanbul, Turkey

Abstract

Self-excited vibration of the tool, regenerative chatter, can be predicted and eliminated if the stability lobe diagram of the spindle–holder–tool assembly is known. Regardless of the approach being used, analytically or numerically, forming the stability lobe diagram of an assembly implies knowing the point frequency response function (FRF) in receptance form at the tool tip. In this paper, it is aimed to study the effects of spindle–holder and holder–tool interface dynamics, as well as the effects of individual bearings on the tool point FRF by using an analytical model recently developed by the authors for predicting the tool point FRF of spindle–holder–tool assemblies. It is observed that bearing dynamics control the rigid body modes of the assembly, whereas, spindle–holder interface dynamics mainly affects the first elastic mode, while holder–tool interface dynamics alters the second elastic mode. Individual bearing and interface translational stiffness and damping values control the natural frequency and the peak of their relevant modes, respectively. It is also observed that variations in the values of rotational contact parameters do not affect the resulting FRF considerably, from which it is concluded that rotational contact parameters of both interfaces are not as crucial as the translational ones and therefore average values can successfully be used to represent their effects. These observations are obtained for the bearing and interface parameters taken from recent literature, and will be valid for similar assemblies. Based on the effect analysis carried out, a systematic approach is suggested for identifying bearing and interface contact parameters from experimental measurements.
© 2006 Elsevier Ltd. All rights reserved.

Keywords: Chatter stability; Bearing and interface dynamics; Parametric identification

1. Introduction

Regenerative chatter vibrations develop due to the dynamic interactions between the workpiece and the cutting tool, and result in unstable cutting, poor surface quality and permanent damage on the machine tool itself. The regeneration of waviness is known to be due to the phase between the subsequent cuts on the surface of the workpiece. Stability lobe diagrams supply the spindle speed—axial depth of cut combinations for which this phase is minimized and the cutting process is stable. The basics of chatter theory and stability lobe diagrams were introduced by Tobias [1,3] and Tlusty [2,4] for orthogonal

cutting conditions and time-invariant process dynamics. Merrit [5] used the Nyquist stability criterion of feedback control theory for developing the stability lobe diagrams and obtained similar results, again for orthogonal cutting with time invariant process dynamics. However, the stability analysis of milling is complicated due to the rotation of the cutting tool which results in time varying directional factors and system dynamics. Tlusty [6–8] made time domain simulations for predicting chatter stability in milling. Minis and Yanushevsky [9,10] employed Floquet's theorem and Fourier series for the formulation of milling stability and used Nyquist criterion for the numerical solution. Altintas and Budak [11] presented the analytical model for the stability limits in milling which was shown to be very fast for the generation of stability lobe diagrams [12].

*Corresponding author. Tel.: +90 216 483 9519; fax: +90 216 483 9550.
  E-mail address: ebudak@sabanciuniv.edu (E. Budak).

The common point of the numerical and analytical milling stability models is the fact that they all require the tool point FRF, which is generally denoted by $G(\omega)$. Performing experimental modal analysis by using a low mass accelerometer, instrumented hammer and a spectrum analyzer is a common way of obtaining the tool point FRF. However, any change in the spindle–holder–tool assembly, such as tool and/or holder changes, will affect the system dynamics and a new measurement will be required. This approach may consume considerable amount of time which is costly on production machines since the machine should be stopped for every new measurement, even for the simplest changes in the assembly. In order to reduce experimentation, the receptance coupling theory of structural dynamics has been implemented for modeling the spindle–holder–tool dynamics semi-analytically [13–18]. It is suggested that the dynamics of spindle–holder subassembly can be obtained experimentally at the holder tip for once, then, it can be coupled with the dynamics of the tool, which is obtained analytically by considering the tool as a beam with free end conditions. This semi-analytical approach can give accurate results and save considerable time in practical applications as long as the holder–tool interface dynamics is modeled or experimentally identified accurately. Duncan and Schmitz [19,20] improved the use of receptance coupling approach to handle different holder types using a single experimental measurement. In a recent study, Ertürk et al. [21] presented an analytical model for predicting the tool point FRF, in which they use Timoshenko beam theory, receptance coupling and structural modification techniques for modeling the spindle–holder–tool dynamics. In all these recent studies, the common objective is to minimize experimentation for the prediction of tool point FRF and the common crucial requirement of them is the accurate knowledge of the connection dynamics. By using the new model they suggested, Ertürk et al. [21] have shown that the relative motion between the components (spindle, holder and tool) can be more important than their individual structural motions since the components are non-slender. This result, implicitly points out the importance of the accurate knowledge of interface dynamics for obtaining the tool point FRF correctly in the existing analytical and semi-analytical models.

In classical tool receptance coupling, the interface parameters are iteratively obtained by employing least square error minimization until the model and experimental FRFs are fitted for all the modes appearing in the existing frequency range. In such an approach, any modeling and measurement error will be compensated by the extracted inaccurate or incorrect interface dynamic parameters, and therefore they can successfully be used only for the configuration for which the experimental study is carried out. Consequently, identification of correct contact parameters is an important issue in employing mathematical models. Knowing how spindle–holder and holder–tool interface dynamics affect the resulting tool point FRF will help to identify contact parameters more accurately, and will also make it possible to observe how possible errors in the extracted interface dynamics are reflected on the tool point FRF of the assembly.

In this paper, by using the analytical model developed [21], the effects of bearing and interface dynamics on the tool point FRF are analyzed. From the results of the effect analysis, suggestions are made for developing systematic approaches for the identification of bearing and interface dynamics from experimental measurements. The analytical model developed in the previous study [21] is briefly summarized in the next section.

2. Mathematical modeling

In the model developed, spindle, holder and tool, which are the main system components, are modeled as multi-segment beams by using Timoshenko beam theory. The individual multi-segment components (spindle, holder and tool) are formed by coupling the end point receptances of uniform beams rigidly. Determination of the end point receptances of a uniform Timoshenko beam with free end conditions is given in [21] in detail.

Consider the rigid coupling of two uniform beams as shown in Fig. 1. Using the formulation presented in [21], the end point receptance matrices of beams A and B can be obtained as

$$[A] = \begin{bmatrix} [A_{11}] & [A_{12}] \\ [A_{21}] & [A_{22}] \end{bmatrix}, \tag{1}$$

$$[B] = \begin{bmatrix} [B_{11}] & [B_{12}] \\ [B_{21}] & [B_{22}] \end{bmatrix}, \tag{2}$$

where submatrices of the above matrices include the point and transfer receptance functions of the segment end points. For example, the point receptance matrix of node $A1$ in beam A is given as

$$[A_{11}] = \begin{bmatrix} H_{A1A1} & L_{A1A1} \\ N_{A1A1} & P_{A1A1} \end{bmatrix}. \tag{3}$$

Note that $[A_{11}]$ actually represents $[A_{A1A1}]$, and just for simplicity it is written in the following formulation as $[A_{11}]$ (the same is true for other receptance matrices). The receptance functions, which are denoted by letters H, N, L
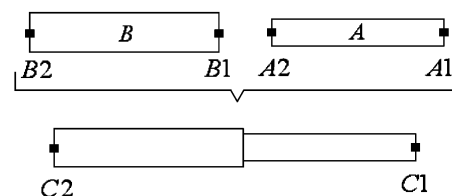

Fig. 1. Rigid coupling of two uniform beams with free end conditions.

and P, are defined as follows:

$$y_j = H_{jk}f_k, \quad \theta_j = N_{jk}f_k,$$
$$y_j = L_{jk}m_k, \quad \theta_j = P_{jk}m_k, \tag{4}$$

where y and θ represent the linear and angular displacements, respectively, and f and m are the forces and the moments, respectively, applied at the points of interest (j and k). Similarly, the other point and transfer receptance matrices can be expressed for segments A and B. Then, by using rigid receptance coupling, the receptance matrix of two-segment beam C can be obtained:

$$[C] = \begin{bmatrix} [C_{11}] & [C_{12}] \\ [C_{21}] & [C_{22}] \end{bmatrix}, \tag{5}$$

where

$$[C_{11}] = [A_{11}] - [A_{12}][[A_{22}] + [B_{11}]]^{-1}[A_{21}], \tag{6}$$

$$[C_{12}] = [A_{12}][[A_{22}] + [B_{11}]]^{-1}[B_{12}], \tag{7}$$

$$[C_{21}] = [B_{21}][[A_{22}] + [B_{11}]]^{-1}[A_{21}], \tag{8}$$

$$[C_{22}] = [B_{22}] - [B_{21}][[A_{22}] + [B_{11}]]^{-1}[B_{12}]. \tag{9}$$

By following the same formulation, one might continue coupling more segments like a chain to form an n-segment beam with the same boundary conditions (free–free) as illustrated in Fig. 2.

In order to include the dynamics of bearings, the structural modification technique presented by Özgüven [22] is used in the model. For instance, in order to obtain the end point FRFs of the spindle shown in Fig. 3, starting from the right end, one might couple the two segments at the right side of the bearing through Eqs. (6)–(9) as depicted in Fig. 4. Having obtained the two-segment beam
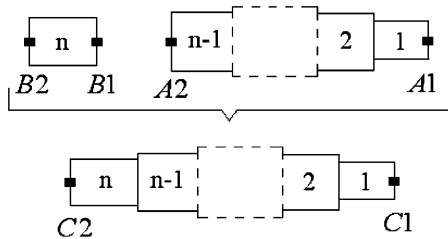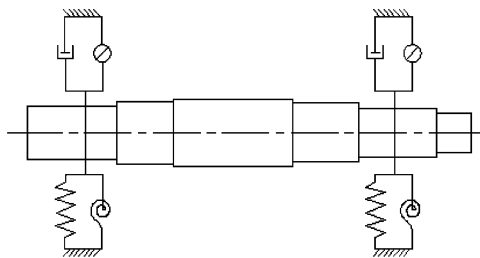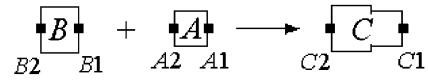

Fig. 2. Rigid coupling of n-th segment.

Fig. 3. A simple spindle model: multi-segment beam grounded by springs and dampers.

Rigid Receptance Coupling:
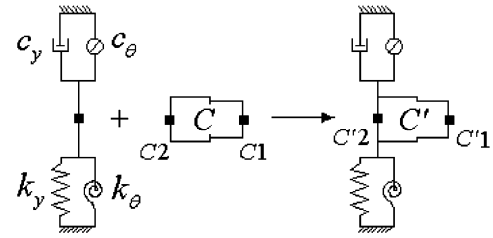

Structural Modification:

Fig. 4. Receptance coupling of two segments and addition of bearing dynamics to the system by structural modification.

C, it is now possible to add the bearing dynamics to beam C as springs and dampers in order to form system C'. Before structural modification, the elements of matrix $[C]$ should be rearranged such that

$$[\alpha_C] = \begin{bmatrix} H_{C1C1} & H_{C1C2} & L_{C1C1} & L_{C1C2} \\ H_{C2C1} & H_{C2C2} & L_{C2C1} & L_{C2C2} \\ N_{C1C1} & N_{C1C2} & P_{C1C1} & P_{C1C2} \\ N_{C2C1} & N_{C2C2} & P_{C2C1} & P_{C2C2} \end{bmatrix}. \tag{10}$$

Then, the receptance matrix of the modified system, $[\alpha_{C'}]$, is given by

$$[\alpha_{C'}] = [[I] + [\alpha_C][D]]^{-1}[\alpha_C], \tag{11}$$

where $[I]$ is the identity matrix and $[D]$ is the dynamic structural modification matrix which includes the translational and rotational, stiffness and damping information of the bearing:

$$[D] = \begin{bmatrix} 0 & 0 & 0 & 0 \\ 0 & k_y + i\omega c_y & 0 & 0 \\ 0 & 0 & 0 & 0 \\ 0 & 0 & 0 & k_\theta + i\omega c_\theta \end{bmatrix}. \tag{12}$$

The efficiency of this modification technique can be increased by effective arrangement of the elements of matrix $[D]$ such that the size of the non-zero submatrix is minimum. The dynamic structural modification matrix can simply be rearranged so that Eq. (11) can be written as partitioned matrices [22] and this way the size of the matrix to be inverted reduces from 4 to 2 as shown in [21]. Note that, the rotational interface dynamics terms in Eq. (12) vanish ($k_\theta = c_\theta = 0$), since generally spindle bearings are self-aligning and they do not carry moment.

The remaining segments of the spindle shown in Fig. 3 can now be coupled and the other bearing can be added to the system in a similar manner to obtain the end point FRFs of the spindle. Using the procedure explained above, end point FRFs of spindle, holder and tool can be found.

Then, the final step is to couple these main system components to obtain the tool point FRF. However, these components should be coupled elastically due to the flexibility and damping introduced by the contacts at spindle–holder and holder–tool interfaces. Therefore, the coupling expressions of the components will be slightly different from the rigid coupling expressions of the segments given by Eqs. (6)–(9). When the end point receptances of the spindle on bearings (S) are coupled with those of the holder (H), the end point receptance matrices of the spindle–holder (SH) assembly can be obtained from:

$$[SH_{11}] = [H_{11}] - [H_{12}][[H_{22}] + [K_{sh}]^{-1} + [S_{11}]]^{-1}[H_{21}],$$
(13)

$$[SH_{12}] = [H_{12}][[H_{22}] + [K_{sh}]^{-1} + [S_{11}]]^{-1}[S_{12}],$$
(14)

$$[SH_{21}] = [S_{21}][[H_{22}] + [K_{sh}]^{-1} + [S_{11}]]^{-1}[H_{21}],$$
(15)

$$[SH_{22}] = [S_{22}] - [S_{21}][[H_{22}] + [K_{sh}]^{-1} + [S_{11}]]^{-1}[S_{12}].$$
(16)

Here, $[K_{sh}]$ is the complex stiffness matrix representing spindle–holder interface dynamics:

$$[K_{sh}] = \begin{bmatrix} k_y^{sh} + i\omega c_y^{sh} & 0 \\ 0 & k_\theta^{sh} + i\omega c_\theta^{sh} \end{bmatrix},$$
(17)

where k_y^{sh} is the translational stiffness, c_y^{sh} is the translational damping, k_θ^{sh} is the rotational stiffness and c_θ^{sh} is the rotational damping at the spindle–holder interface. Finally, the tool (T) can be added to the spindle–holder (SH) system to obtain the end point FRFs of spindle–holder–tool (SHT) assembly. The FRF required for the stability lobe diagram of a given spindle–holder–tool assembly is the one that gives the relation between the transverse displacement and force at the tool tip, which is the first element of the following matrix:

$$[SHT_{11}] = [T_{11}] - [T_{12}][[T_{22}] + [K_{ht}]^{-1} + [SH_{11}]]^{-1}[T_{21}],$$
(18)

where $[K_{ht}]$ is the complex stiffness matrix of the holder–tool interface dynamics

$$[K_{ht}] = \begin{bmatrix} k_y^{ht} + i\omega c_y^{ht} & 0 \\ 0 & k_\theta^{ht} + i\omega c_\theta^{ht} \end{bmatrix}.$$
(19)

In Eq. (19), k_y^{ht} is the translational stiffness, c_y^{ht} is the translational dampinpg, k_θ^{ht} is the rotational stiffness and c_θ^{ht} is the rotational damping at the holder–tool interface.

Note that, an alternative approach in coupling segments rigidly or coupling components elastically would be to use impedance coupling. However, impedance coupling requires dealing with matrices of higher dimensions as the dynamic information of all connection points are kept in the resulting system impedance matrix [23].

3. Effect analysis

In this section, first the tool point FRF of a typical spindle–holder–tool assembly will be obtained by using the analytical model developed, and then, the effects of bearing and interface dynamics on the resulting tool point FRF will be studied in detail through a case study. For convenience, the assembly used in [21] will be used here as the example system for the effect analysis.

3.1. Prediction of tool point FRF

Fig. 5 shows the spindle–holder–tool combination used in this case study. The geometric properties of the components and the dynamic properties of the bearings and interfaces are given in Tables 1–3. Regarding the material properties, all components are taken as steel with mass density $\rho = 7800\,kg/m^3$, Young's modulus $E = 200\,GPa$, Poisson's ratio $v = 0.3$ and the material loss factor is assumed to be $\gamma = 0.003$. Typical values are taken for the bearing and interface dynamics from the related literature. Numerical values identified in a recent study [24] are used for bearing and spindle–holder interface dynamics, and for the holder–tool interface dynamics, the values given in Refs. [13,14] are used. The magnitude diagram of the tool point FRF, $G(\omega)$, obtained by using the model developed is shown in Fig. 6 together with its phase diagram. Note that the resulting tool point FRF can now directly be used in the analytical model presented by Budak et al. [12] and the stability lobe diagram of the given spindle–holder–tool combination (Fig. 5) can be obtained to determine the stable spindle speed–axial depth of cut combinations. However, in this paper, the objective is to use the model developed to investigate the effects of bearing and interface dynamics on the tool point FRF. Results of this analysis can be used in spindle design and holder selection as well as in determining contact stiffness and damping values for spindle–holder and holder–tool interfaces from experimental FRF measurements.
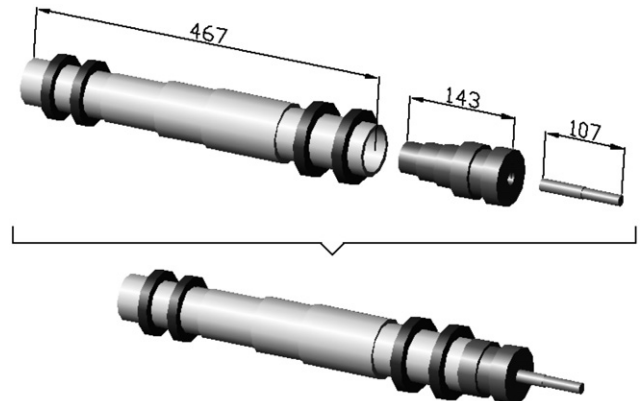

Fig. 5. Components of the example system used for the effect analysis and their assembly.

Table 1
Component dimensions[a]: (a) Spindle; (b) Holder; (c) Tool

(a) Spindle dimensions										
Segment number	1	2	3	4	5	6	7	8	9	10
Length (mm)	26	26	26	38	100	66	75	30	40	40
Outer diameter (mm)	66	66	66	66	76	70	62	58	58	58
Inner diameter (mm)	54	48	40	32	32	32	32	32	32	32
(b) Holder dimensions										
Segment number	1	2	3	4	5	6				
Length (mm)	22	19	24	26	26	26				
Outer diameter (mm)	72	60	70	54	48	40				
Inner diameter (mm)	16	16	16	16	16	16				
(c) Tool dimensions[b]										
Segment number	1	2								
Length (mm)	50	57								
Outer diameter (mm)	14	16								
Inner diameter (mm)	0	0								

[a]Component segments are numbered starting from the right end of their given figures.
[b]The overhang length of the tool is 85 mm for the given combination.

Table 2
Average dynamical properties of the bearings and interfaces

	Translational stiffness (N/m)	Rotational stiffness (Nm/rad)
Front bearings (for each)	7.5×10^5	—
Rear bearings (for each)	2.5×10^6	—
Spindle–holder interface	5×10^7	1.5×10^6
Holder–tool interface	2×10^7	1.5×10^6

Table 3
Distances of the bearings measured from the right end of the spindle

Bearing no.[a]	Bearing 1	Bearing 2	Bearing 3	Bearing 4
Distance (mm)	26	78	387	427

[a]The bearings are numbered starting from the right end of the spindle.

3.2. Effect of bearing dynamics on the tool point FRF

In order to study the effects of bearing dynamics on the tool point FRF, first the same stiffness values are used for each of two front bearings (7.5×10^5 N/m) and for each of two rear bearings (2.5×10^6 N/m). Stiffness values of the bearings are first increased and then decreased 50% of their original values, and the results are shown in Fig. 7. Damping values of the bearings are taken to be very low (light damping) since they do not affect the natural frequencies. As can be seen from the figure, the bearing stiffness values have a considerable effect on the first two modes of the system which are the rigid body modes, whereas, they have almost no effect on the remaining (elastic) modes, as also observed in a recent study [24] which uses finite element method (FEM) and experimentation for a spindle–holder assembly. Here, it is also possible to study the individual effects of the front and rear
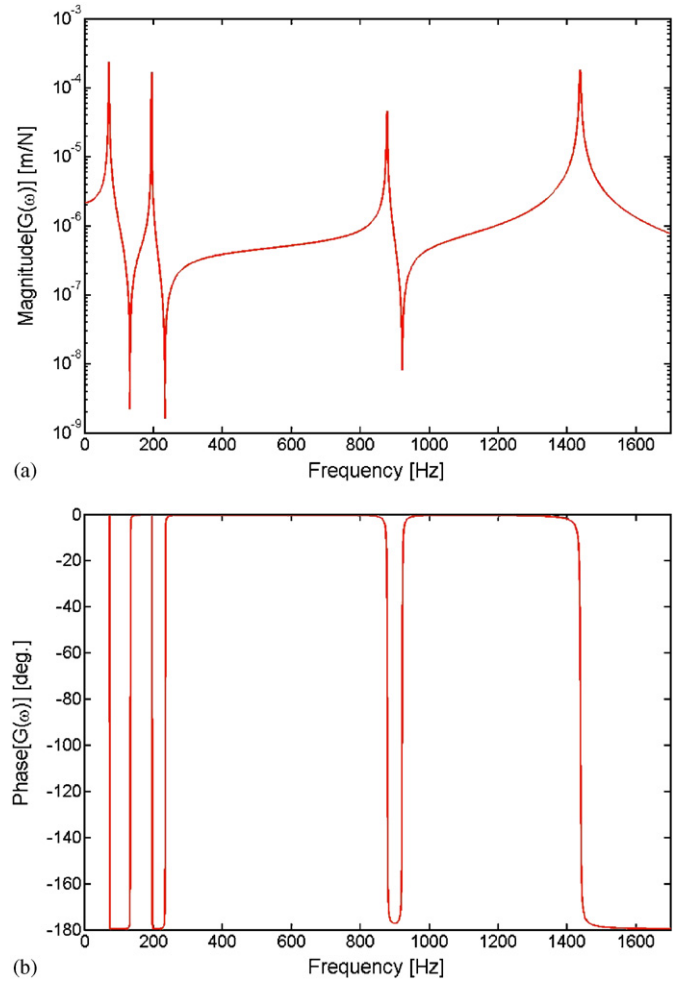
Fig. 6. Tool point FRF $G(\omega)$ of the assembly: (a) magnitude diagram; (b) phase diagram.

bearings: Fig. 8 shows the change in $G(\omega)$ due to the variation in the front bearing stiffness values when the rear bearing stiffness values are kept constant at their average
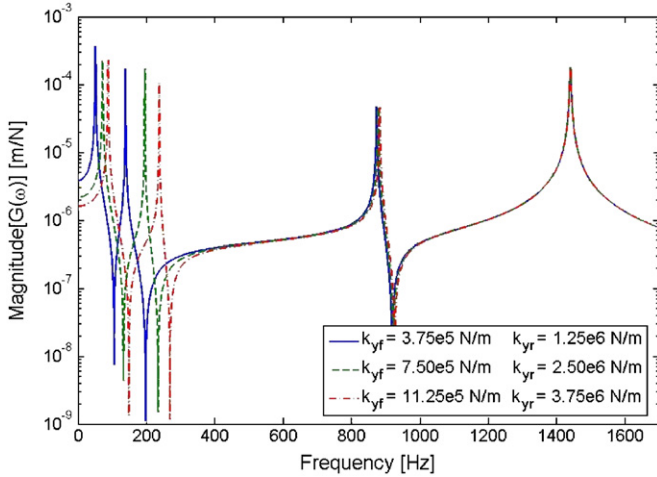
Fig. 7. The combined effect of bearing stiffness values on the tool point FRF.
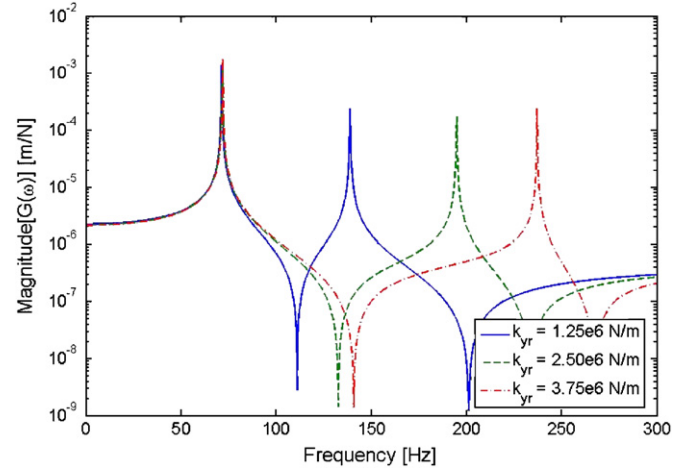

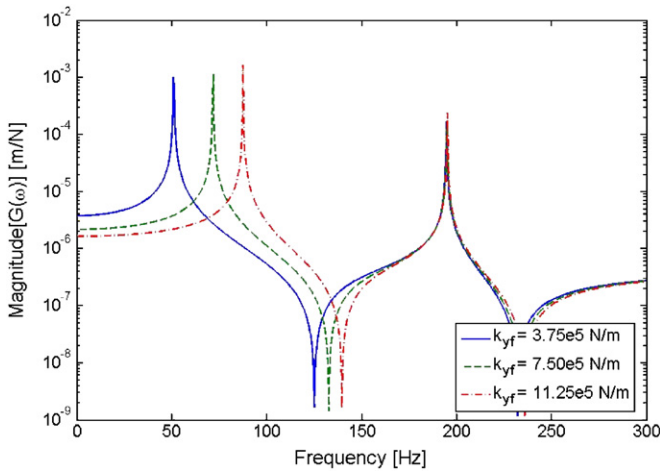Fig. 9. The effect of stiffness values of the rear bearings on the tool point FRF.

Fig. 8. The effect of stiffness values of the front bearings on the tool point FRF.

values. It is observed that the dynamics of the front bearings primarily control the first rigid body mode. When the stiffness values of the front bearings are kept at their average values, and the stiffness values of the rear bearings are varied by the same percentage (Fig. 9), it is observed that the rear bearings mainly affect the second rigid body mode. It is an expected result for the front bearings to affect the first mode and the rear bearing to affect the second mode, as the front bearings are softer and the rear bearing are stiffer; but it is more interesting to observe that the rear bearings do not affect the first mode at all, and similarly front bearings do not affect the second mode almost at all. Therefore, for the system used, the spindle geometry and bearing properties (i.e. dimensions of the shaft, and bearing types and locations) have the most important effect on the first two modes. This also implies at this stage that if chatter develops in one of the first two modes, changing the holder or the tool may not help to avoid it, which will be verified in the following sections. A

more rigid or flexible holder and/or tool will slightly alter these modes, just because of the change in the total mass of the assembly, rather than the change in the flexural rigidity obtained by the new tool and/or holder. For instance, a new holder with higher bending rigidity and higher mass will slightly reduce the frequencies of the rigid body modes, just because of an additional mass effect.

3.3. Effect of spindle–holder interface dynamics on the tool point FRF

In a very similar way, sensitivity of tool point FRF to the spindle–holder interface dynamics is studied in this section. As the variations of the interface damping do not affect the natural frequencies, light damping is assumed. The translational and rotational stiffness values are first halved and then doubled with respect to their average values. Fig. 10 shows the effect of the translational stiffness on tool point FRF, when the rotational stiffness is kept constant. It is observed that the translational stiffness at the spindle–holder interface dominantly affects the first elastic mode of the FRF. The second elastic mode is not that much affected, and the change in this interface parameter has no effect on the natural frequencies of the rigid body modes. Regarding the effect of rotational stiffness of the same interface, the value of this parameter is first changed to 0.75×10^6 Nm/rad and then to 2.25×10^6 Nm/rad, and the results for three different values of the rotational stiffness are shown in Fig. 11. It can be seen from the figure that the variations in the rotational stiffness of spindle–holder interface has almost negligible effect on the FRF, compared with the effect of the translational stiffness for the same percentage of variation. This shows that the rotational stiffness value of the spindle–holder interface with the order of magnitude 10^6 Nm/rad is quite high, as a result of which, variation around this highly stiff value almost does not affect the resulting FRF. If the rotational stiffness of this interface is at this order of magnitude, it
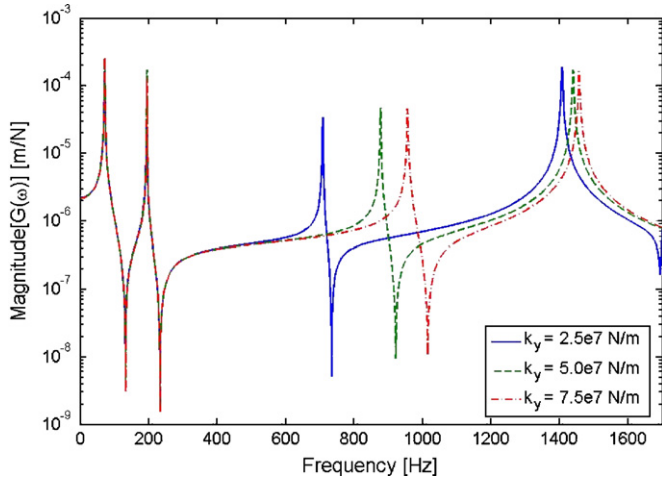
Fig. 10. The effect of translational stiffness at the spindle–holder interface on the tool point FRF.
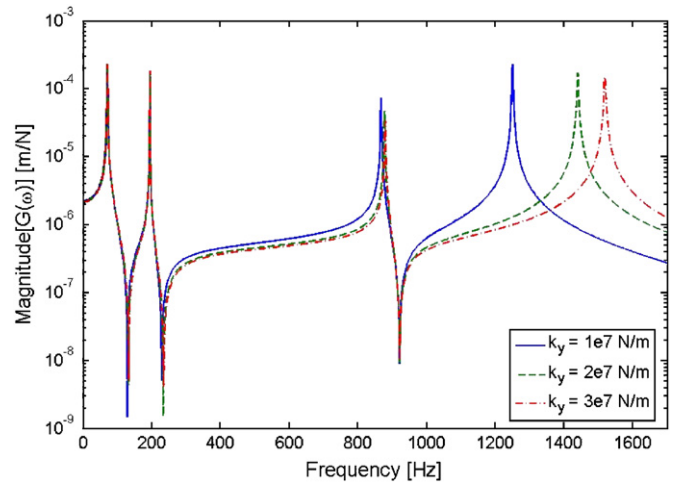

Fig. 12. The effect of translational stiffness at the holder–tool interface on the tool point FRF.
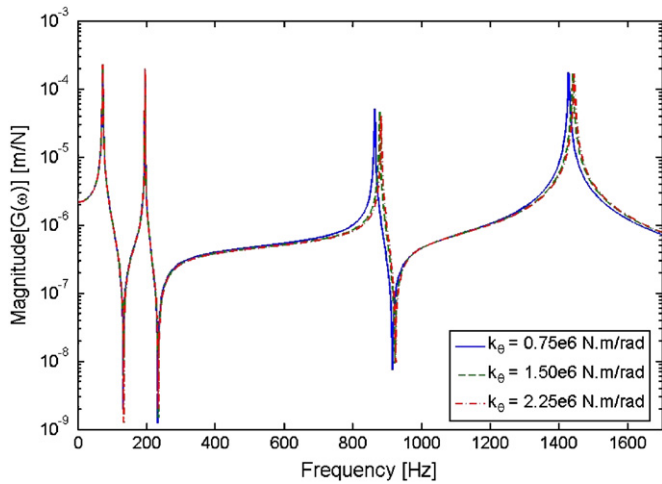

Fig. 11. The effect of rotational stiffness at the spindle–holder interface on the tool point FRF.
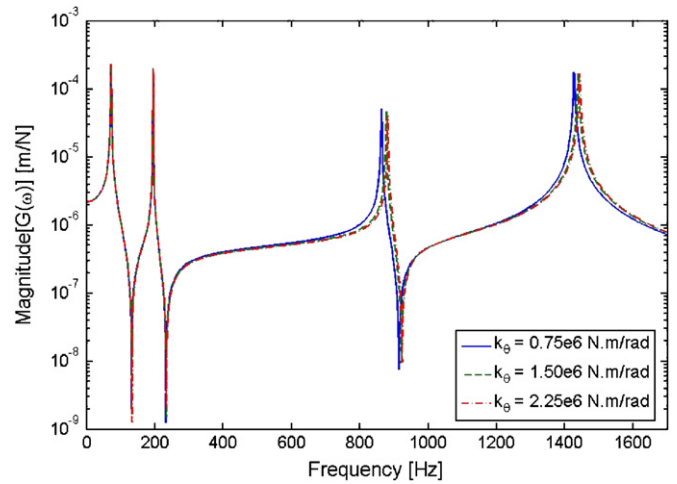

Fig. 13. The effect of rotational stiffness at the holder–tool interface on the tool point FRF.

can be concluded that the accurate identification of this parameter for prediction of the tool point FRF is not so crucial, and using an average value will not alter the stability lobe diagram considerably.

3.4. Effect of holder–tool interface dynamics on the tool point FRF

The same percentage of variation ($\pm 50\%$) is applied on the translational and rotational stiffness values representing holder–tool interface in order to study the sensitivity of FRF to the holder–tool interface dynamics. The rotational stiffness value is kept constant while the translational stiffness is varied (Fig. 12), and it is observed that the translational stiffness strongly controls the second elastic mode, whereas its effect on the first elastic mode is not considerable. When the translational stiffness of this interface is kept constant at its average value and the rotational stiffness is varied, from the resulting tool point

FRF (Fig. 13) it can be concluded that, being very similar to the case of the spindle–holder interface, the rotational stiffness at this connection has negligible effect on FRF. This is again due to the fact that the rotational stiffness value in the order of 10^6 Nm/rad is very high, i.e. the rotational connection is highly rigid, so that variation of rotational stiffness does not alter the tool point FRF considerably. Furthermore, it is observed that the dynamics of holder–tool interface does not affect the rigid body modes of the assembly.

Therefore, the observations made so far indicate that, for the first elastic mode, spindle–holder interface is the most important link in the chain, whereas the same is true for holder–tool interface for the second elastic mode in this case study. These observations together with the conclusion that the rotational springs at the interfaces do not have significant effects on the system dynamics (as long as they have nominal values in the orders quoted above) provide very useful information for the

identification of the interface parameters as will be discussed in Section 3.6.

3.5. Effect of bearing and interface damping values on the tool point FRF

Up to this point, bearing and interface damping values have been set to values close to zero (i.e. light damping is assumed) since the main consideration was the prediction of natural frequency and the connection damping values would affect only the peak values of the resulting tool point FRF. Now, in order to study the mode at which the peak FRF value is affected from interface damping, a similar analysis is performed by varying the damping values at the connection points. In order to study the effect of contact damping, damping values in a reasonable range are used for the same example system (Fig. 5), where the connection stiffness values are kept at their average values (Table 2). It is observed that the variation of the front bearing damping affects the FRF values at the first rigid body mode; whereas, damping of the rear bearing controls the peak of the second rigid body mode. Translational contact damping at the spindle–holder interface mainly alters the peak value of the first elastic mode and the effect of rotational damping at the same interface is negligible when compared with the effect of translational damping. Similarly, when the damping values of the holder–tool interface are varied, it is observed that the translational damping controls the peak of the second elastic mode and the rotational damping has again negligible effect on the tool point FRF. As a sample for damping effect analysis, variations of the tool point FRF due to the changes in holder–tool interface translational and rotational damping values are depicted in Figs. 14 and 15, respectively. In order to see the variation in the magnitudes better, linear scale is used for the magnitude axis. When the translational damping of this interface is increased by a factor of 4, peak value of the second elastic mode is decreased almost by a factor of 3;
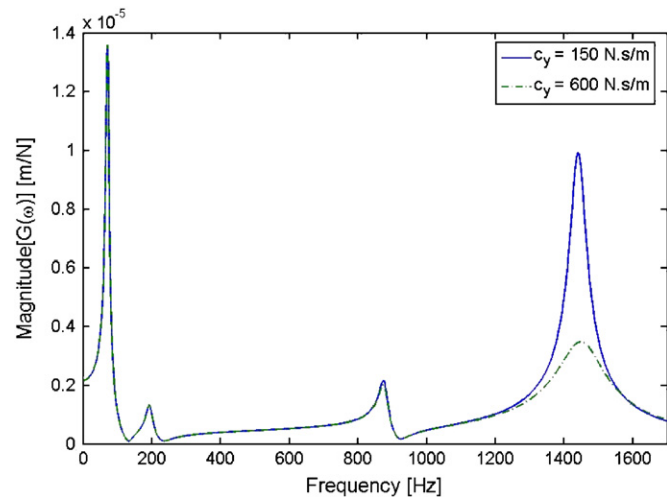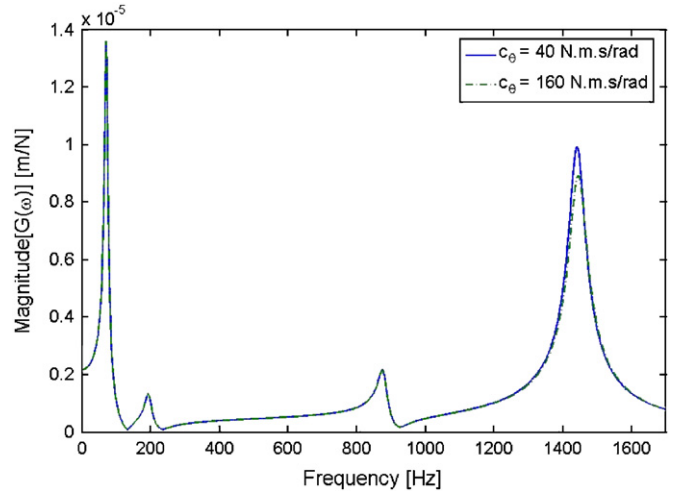

Fig. 15. The effect of rotational damping at the holder–tool interface on the tool point FRF.

whereas, the first elastic mode as well as the rigid body modes are not affected (Fig. 14). When the rotational damping of this interface is increased by the same factor, however, it is observed that the change in the resulting FRF is very slight (Fig. 15). From the damping effect analysis, it can be concluded that the rotational contact damping values are not as crucial as the translational ones for a correct tool point FRF, and average values can be used for the order of magnitudes used in this case study.

3.6. Use of effect analysis in identification of connection parameters

The results of the effect analysis which base on the case study given here, show that the dynamics of the bearings directly control the first two modes (the rigid body modes) of the tool point FRF, $G(\omega)$. They also demonstrate that the dynamics of the front bearings (which are softer) mainly affect the first rigid body mode; whereas, those of the rear bearings control the second rigid body mode. Furthermore, the translational stiffness and damping at the spindle–holder interface mainly control the first elastic mode; whereas, the translational stiffness and damping at the holder–tool interface strongly affect the second elastic mode. One other important result is that, for the order of magnitudes of the numerical values obtained from the literature [13,14], the variations in the rotational stiffness and damping values of both interfaces have negligible effect on $G(\omega)$ when compared with the effects of the variations in the translational stiffness and damping values of the same interfaces. It may be possible to generalize the above observations for spindle–holder–tool assemblies that have similar geometry and dynamics. However, for different geometries and/or dynamic properties, a similar theoretical analysis has to be carried out to determine which mode is controlled by which connection parameter.

Fig. 14. The effect of translational damping at the holder–tool interface on the tool point FRF.

The above conclusions can be used in parametric identification of connection dynamics of a given spindle–holder–tool assembly from experimental measurement of tool point receptance much more easily and accurately compared to previous approaches used. Having the information of which connection parameters affect which mode, identification should be performed by extracting the parameters of interest from their relevant modes.

4. Conclusions

In this paper, the analytical method presented in a recent study for modeling spindle–holder–tool assemblies and predicting the tool point FRF is summarized; and using this model, the effects of bearing and interface dynamics on the tool point FRF are studied for a typical case example. The details of the formulation and the validation of the model that can be used for a wide range of applications from constructing stability lobe diagrams to spindle design, are given in [21]. In this paper, it is intended to make use of this model in studying the effects of spindle–holder and holder–tool contact parameters, as well as individual bearing properties on tool point FRF so that systematic approaches can be found in predicting contact parameters from experimental measurements.

It is observed that variations in the bearing dynamic properties mainly alter the natural frequencies of the rigid body modes (first two modes of the FRF), and moreover they have no considerable effect on the elastic modes of the assembly. When the individual effects of front and rear bearing pairs are studied, it is observed that softer front bearings control the first rigid body mode and stiffer rear bearings control the second rigid body mode, as can be expected. But it is also observed that these two modes are quite uncoupled so that soft bearing stiffness (front pair in the given case study) has almost no effect on second rigid body mode, and vice versa. Thus, it may be concluded that, for a machine tool with a typical spindle, holder and tool assembly similar to the one used in the case study here, the chatter stability limits for the first two modes are almost determined by the spindle and cannot be improved even if the holder and tool rigidities are increased. Therefore, changing the holder and/or tool will have only a very slight "mass effect" on the self-excited vibrations developing in one of these rigid body modes, since the rigid body modes are not affected from the flexural rigidity of the assembly.

The effects of contact parameters (stiffness and damping) at the spindle–holder and holder–tool interfaces on the tool point FRF are also studied. It is observed that the translational stiffness and damping of spindle–holder interface primarily control the first elastic mode of the assembly, whereas, the same parameters of holder–tool interface mainly affect the second elastic mode. It is also observed that the effects of the rotational stiffness and damping values of both interfaces have almost negligible effect compared with the effects of the translational counterparts. Based on these observations, several impor-

tant conclusions can be drawn for contact parameter identification. First of all, since the rotational contact parameters of both interfaces are not as crucial as the translational ones, average values can successfully be used to represent their effects. At this point, it should be noted that it is not suggested here that the rotational parameters are not required to define the interface dynamics or that they can be neglected. What we suggest here is the fact that using average values for rotational contact parameters will not change the accuracy of the resulting FRF significantly. Thus, in contact parameter identification for various tools and holders that are used in a machining center, it will not be required to determine the rotational contact parameters for all combinations. That will not only save us from an additional task, but will also decrease the number of unknowns by a factor of two in contact parameter identification, and it will increase the computational efficiency considerably. Note that, these observations and conclusions are for the orders of magnitudes of the bearing and interface dynamic parameters taken from the literature. The effects of interface dynamic parameters may differ for numerical values with considerably different orders of magnitudes.

The results of this study suggest that the above effect analysis can be used in developing an identification procedure for the translational contact parameters of each interface. After performing an effect analysis for a given assembly, the mode-interface relations can be obtained and the dynamic parameters of each interface can be identified by using its relevant mode. Even the stiffness and damping values of spindle bearings can be identified more accurately and more easily by using the approach suggested here. Accurate identification of contact parameters seems to be a must to be able to use the mathematical model employed in this study, as well as any similar model, for predicting chatter stability of machining centers.

Acknowledgments

References

[1] S.A. Tobias, W. Fishwick, The chatter of lathe tools under orthogonal cutting conditions, Transactions of ASME 80 (1958) 1079–1088.
[2] J. Tlusty, M. Polacek, The stability of machine tools against self-excited vibrations in machining, Proceedings of the ASME International Research in Production Engineering, Pittsburgh, LA, USA, 1963, pp. 465–474.
[3] S.A. Tobias, Machine Tool Vibration, Blackie and Sons Ltd, 1965.
[4] F. Koenisberger, J. Tlusty, Machine Tool Structures—vol. I: Stability Against Chatter, Pergamon Press, Englewood Cliffs, NJ, 1967.
[5] H. Merrit, Theory of self-excited machine tool chatter, Transactions of ASME Journal of Engineering for Industry 87 (1965) 447–454.
[6] J. Tlusty, F. Ismail, Basic nonlinearity in machining chatter, Annals of the CIRP 30 (1981) 21–25.

[7] J. Tlusty, Dynamics of high-speed milling, Transactions of ASME Journal of Engineering for Industry 108 (2) (1986) 59–67.

[8] S. Smith, J. Tlusty, Efficient simulation programs for chatter in milling,, Annals of the CIRP 42 (1) (1993) 463–466.

[9] I. Minis, T. Yanushevsky, R. Tembo, R. Hocken, Anaylsis of linear and nonlinear chatter in milling, Annals of the CIRP 39 (1990) 459–462.

[10] I. Minis, T. Yanushevsky, A new theoretical approach for prediction of machine tool chatter in milling, ASME Journal of Engineering for Industry 115 (1993) 1–8.

[11] Y. Altintas, E. Budak, Analytical prediction of stability lobes in milling, Annals of the CIRP 44 (1995) 357–362.

[12] E. Budak, Y. Altintas, Analytical prediction of chatter stability in milling—part I: general formulation; part II: application to common milling systems, Transactions of ASME, Journal of Dynamic Systems, Measurement, and Control 120 (1998) 22–36.

[13] T. Schmitz, R. Donaldson, Predicting high-speed machining dynamics by substructure analysis, Annals of the CIRP 49 (1) (2000) 303–308.

[14] T. Schmitz, M. Davies, M. Kennedy, Tool point frequency response prediction for high-speed machining by RCSA, ASME Journal of Manufacturing Science and Engineering 123 (2001) 700–707.

[15] T. Schmitz, M. Davies, K. Medicus, J. Synder, Improving high-speed machining material removal rates by rapid dynamic analysis, Annals of the CIRP 50 (1) (2001) 263–268.

[16] T. Schmitz, T. Burns, Receptance coupling for high-speed machining dynamics prediction, Proceedings of the 21st International Modal Analysis Conference, February 3–6, 2003, Kissimmee, FL (on CD).

[17] S.S. Park, Y. Altintas, M. Movahhedy, Receptance coupling for end mills, International Journal of Machine Tools and Manufacture 43 (2003) 889–896.

[18] E.B. Kivanc, E. Budak, Structural modeling of end mills for form error and stability analysis, International Journal of Machine Tools and Manufacture 44 (2004) 1151–1161.

[19] G.S. Duncan, T. Schmitz, An improved RCSA model for tool point frequency response prediction, Proceedings of the 23rd International Modal Analysis Conference, January 30–February 3, 2005, Orlando, FL (on CD).

[20] T. Schmitz, G.S. Duncan, Three-component receptance coupling substructure analysis for tool point dynamics prediction, ASME Journal of Manufacturing Science and Engineering 127 (2005) 781–790.

[21] A. Ertürk, H. N. Özgüven, E. Budak, Analytical modeling of spindle–tool dynamics on machine tools using Timoshenko beam model and receptance coupling for the prediction of tool point FRF, International Journal of Machine Tools and Manufacture, in press, doi:10.1016/j.ijmachtools.2006.01.032.

[22] H.N. Özgüven, A new method for harmonic response of non-proportionally damped structures using undamped modal data, Journal of Sound and Vibration 117 (1987) 313–328.

[23] A. Ertürk, E. Budak, H.N. Özgüven, Dynamic modeling of spindle–tool holder–tool assembly in machining centers, Proceedings of 12th National Symposium on Theory of Machines, vol. I, June 9–11, Kayseri, Turkey, 2005, pp. 15–26 (in Turkish).

[24] N. Arakere, T. Schmitz, C. Cheng, Rotor dynamic response of a high-speed machine tool spindle, Proceedings of the 23rd International Modal Analysis Conference, January 30–February 3, 2005, Orlando, FL (on CD).